

# Accurate characterization of the stellar and orbital parameters of the exoplanetary system WASP-33 b from orbital dynamics

L. Iorio<sup>1\*</sup>

<sup>1</sup>*I Ministero dell'Istruzione, dell'Università e della Ricerca (M.I.U.R.), Viale Unità di Italia 68 Bari, (BA) 70125, Italy*

26 October 2021

## ABSTRACT

By using the most recently published Doppler tomography measurements and accurate theoretical modeling of the oblateness-driven orbital precessions, we tightly constrain some of the physical and orbital parameters of the planetary system hosted by the fast rotating star WASP-33. In particular, the measurements of the orbital inclination  $i_p$  to the plane of the sky and of the sky-projected spin-orbit misalignment  $\lambda$  at two epochs about six years apart allowed for the determination of the longitude of the ascending node  $\Omega$  and of the orbital inclination  $I$  to the apparent equatorial plane at the same epochs. As a consequence, average rates of change  $\dot{\Omega}_{\text{exp}}$ ,  $\dot{I}_{\text{exp}}$  of this two orbital elements, accurate to a  $\approx 10^{-2}$  deg yr<sup>-1</sup> level, were calculated as well. By comparing them to general theoretical expressions  $\dot{\Omega}_{J_2}$ ,  $\dot{I}_{J_2}$  for their precessions induced by an oblate star whose symmetry axis is arbitrarily oriented, we were able to determine the angle  $i^*$  between the line of sight the star's spin  $S^*$  and its first even zonal harmonic  $J_2^*$  obtaining  $i^* = 142_{-11}^{+10}$  deg,  $J_2^* = (2.1_{-0.5}^{+0.8}) \times 10^{-4}$ . As a by-product, the angle between  $S^*$  and the orbital angular momentum  $L$  is as large as about  $\psi \approx 100$  deg ( $\psi^{2008} = 99_{-4}^{+5}$  deg,  $\psi^{2014} = 103_{-4}^{+5}$  deg), and changes at a rate  $\dot{\psi} = 0.7_{-1.6}^{+1.5}$  deg yr<sup>-1</sup>. The predicted general relativistic Lense-Thirring precessions, or the order of  $\approx 10^{-3}$  deg yr<sup>-1</sup>, are, at present, about one order of magnitude below the measurability threshold.

**Key words:** stars: planetary systems–gravitation–celestial mechanics

## 1 INTRODUCTION

Steady observations of a test particle orbiting its primary over time intervals much longer than its orbital period  $P_b$  can reveal peculiar cumulative features of its orbital motion which may turn out to be valuable tools to either put to the test fundamental theories or characterize the physical properties of the central body acting as source of the gravitational field. It has been just the case so far in several different astronomical and astrophysical scenarios ranging, e.g., from the early pioneering determinations of the multipole moments of the non-central gravitational potential of the Earth with artificial satellites (Kozai 1961; King-Hele 1962; Cook 1962) to the celebrated corroborations of the Einsteinian General Theory of Relativity (GTR) with the explanation of the anomalous (at that time) perihelion precession of Mercury (Einstein 1915)-observationally known since decades (Le Verrier 1859)-, several binary systems hosting at least one emitting pulsar (Hulse & Taylor 1975; Burgay et al. 2003; Lyne et al. 2004; Kramer et al. 2006), and Earth's satellites (Lucchesi & Peron 2010, 2014) implementing earlier ideas put forth since the dawn of the space era and beyond (Lapaz 1954; Cugusi & Proverbio 1978). Plans exist to use in a similar way the stars revolving around the supermassive black hole in Sgr A\* (Ghez et al.

2008; Gillessen et al. 2009; Angéllil, Saha & Merritt 2010; Zhang, Lu & Yu 2015).

With over<sup>1</sup> 1500 planets discovered so far and counting (Han et al. 2014), most of which orbiting very close to their parent stars (Howard 2013), extrasolar systems (Perryman 2014), in principle, represent ideal probes to determine or, at least, constrain some physical parameters of their stellar partners through their orbital dynamics. One of them is the quadrupole mass moment  $J_2$ , accounting for the flattening of the star. It is connected with fundamental properties of the stellar interior such as, e.g., the non-uniform distribution for both velocity rates and mass (Rozelot, Damiani & Pireaux 2009; Damiani et al. 2011; Rozelot & Damiani 2011; Rozelot & Fazel 2013). Also GTR may turn out a valuable goal for exoplanets' analysts also from a practical point of view. Indeed, by assuming its validity, it may be used as a tool for dynamically characterizing the angular momentum  $S$  of the host stars via the so-called Lense-Thirring effect (Lense & Thirring 1918). Such a dynamical variable is able to provide relevant information about the inner properties of stars and their activity. Furthermore, it plays the role of an important diagnostic for putting to the test theories of stellar formation. The angular momentum can also have a crucial

\* E-mail: lorenzo.iorio@libero.it

<sup>1</sup> See, e.g., <http://exoplanets.org/> on the WEB.

impact in stellar evolution, in particular towards the higher mass (Tarafdar & Vardya 1971; Wolff, Edwards & Preston 1982; Vigneron et al. 1990; Wolff & Simon 1997; Herbst & Mundt 2005; Jackson, MacGregor & Skumanich 2005). As a naive measure of the relevance of the Einsteinian theory of gravitation in a given binary system characterized by mass  $M$ , proper angular momentum  $S$  and extension  $r$ , the magnitude of the ratios of some typical gravitational lengths to  $r$  can be assumed. By taking (Bertotti, Farinella & Vokrouhlick 2003)

$$r_M = \frac{GM}{c^2}, \quad (1)$$

$$r_S = \frac{S}{Mc}, \quad (2)$$

where  $G$  and  $c$  are the Newtonian gravitational constant and the speed of light in vacuum, respectively, it can be easily noted that, for exoplanets hosted by Sun-like stars at, say,  $r = 0.005$  au, Eqs 1 to 2 yield

$$\frac{r_M}{r} = 2 \times 10^{-6}, \quad (3)$$

$$\frac{r_S}{r} = 4 \times 10^{-7}. \quad (4)$$

Such figures are substantially at the same level of, or even larger than those of the double pulsar (Burgay et al. 2003; Lyne et al. 2004; Kramer et al. 2006), for which one has

$$\frac{r_M}{r} = 4 \times 10^{-6}, \quad (5)$$

$$\frac{r_S}{r} = 8 \times 10^{-8}. \quad (6)$$

It shows that, in principle, some of the extrasolar planetary systems may well represent important candidates to perform also tests of relativistic orbital dynamics.

In the present work, we will deal with WASP-33 b (Collier Cameron et al. 2010). It is a planet closely transiting a fast rotating and oblate main sequence star along a circular, short-period ( $P_b = 1.21$  d) orbit which is highly inclined to the stellar equator. In Iorio (2011b) it was suggested that, in view of the relatively large size of some classical and general relativistic orbital effects, they could be used to better characterize its parent star as long as sufficient accurate data records were available. It has, now, become possible in view of the latest Doppler tomography measurements processed by Johnson et al. (2015), and of more accurate theoretical models of the orbital precessions involved (Iorio 2011c, 2012).

The plan of the paper is as follows. In Section 2, we illustrate our general analytical expressions for the averaged classical and relativistic precessions of some Keplerian orbital elements in the case of an arbitrary orientation of the stellar symmetry axis and of an unrestricted orbital geometry. Section 3 describes the coordinate system adopted in this astronomical laboratory. Our theoretical predictions of the orbital rates of change are compared to the corresponding phenomenologically measured precessions in Section 4, where tight constraints on some key stellar parameters are inferred, and the perspectives of measuring the Lense-Thirring effect are discussed. Section 5 is devoted to summarizing our findings.

## 2 THE MATHEMATICAL MODEL OF THE ORBITAL PRECESSIONS

A particle at distance  $r$  from a central rotating body of symmetry axis direction  $\hat{S} = \{\hat{S}_x, \hat{S}_y, \hat{S}_z\}$  experiences an additional non-central acceleration (Vrbik 2005)

$$A_{J_2} = -\frac{3GMJ_2R^2}{2r^4} \left\{ \left[ 1 - 5(\hat{r} \cdot \hat{S})^2 \right] \hat{r} + 2(\hat{r} \cdot \hat{S})\hat{S} \right\}, \quad (7)$$

which causes long-term orbital precessions. For a generic orientation of  $\hat{S}$  in a given coordinate system, they were analytically worked out by<sup>2</sup> Iorio (2011c). Among them<sup>3</sup>, we have

$$\begin{aligned} \dot{\Omega}_{J_2} = & \frac{3n_b J_2 R^2}{4a^2 (1-e^2)^2} \left\{ 2\hat{S}_z \cos 2I \csc I (\hat{S}_x \sin \Omega - \hat{S}_y \cos \Omega) + \right. \\ & \left. + \cos I \left[ 1 - 3\hat{S}_z^2 + (\hat{S}_y^2 - \hat{S}_x^2) \cos 2\Omega - 2\hat{S}_x \hat{S}_y \sin 2\Omega \right] \right\}, \quad (8) \end{aligned}$$

$$\begin{aligned} \dot{I}_{J_2} = & -\frac{3n_b J_2 R^2}{2a^2 (1-e^2)^2} (\hat{S}_x \cos \Omega + \hat{S}_y \sin \Omega) \left[ \hat{S}_z \cos I + \right. \\ & \left. + \sin I (\hat{S}_x \sin \Omega - \hat{S}_y \cos \Omega) \right], \quad (9) \end{aligned}$$

which will be relevant for our purposes. In Eqs 8 to 9,  $a$  is the semimajor axis,  $n_b = \sqrt{GMa^{-3}}$  is the Keplerian mean motion,  $e$  is the eccentricity,  $I$  is the inclination of the orbital plane with respect to the coordinate  $\{x, y\}$  plane adopted, and  $\Omega$  is the longitude of the ascending node counted in the  $\{x, y\}$  plane from a reference  $x$  direction to the intersection of the orbital plane with the  $\{x, y\}$  plane itself. Note that if the body's equatorial plane is assumed as  $\{x, y\}$  plane, i.e. if  $\hat{S}_x = \hat{S}_y = 0$ ,  $\hat{S}_z = 1$ , Eqs 8 to 9 reduce to the well known expressions (Bertotti, Farinella & Vokrouhlick 2003)

$$\dot{\Omega}_{J_2}^{(0)} = -\frac{3n_b J_2 R^2}{2a^2 (1-e^2)^2} \cos I, \quad (10)$$

$$\dot{I}_{J_2}^{(0)} = 0; \quad (11)$$

with this particular choice,  $I$  coincides with the angle  $\psi$  between  $S$  and the particle's orbital angular momentum  $L$ . It is important to stress that, in the general case, the cumbersome multiplicative geometrical factor in Equation 8 depending on the spatial orientation of the orbit and of the spin axis does not reduce to  $\cos \psi$ , as it will explicitly turn out clear in Section 3. On the other hand, it can be easily guessed from the fact that  $\cos \psi$  is linear in the components of  $\hat{S}$ , while the acceleration of Equation 7 is quadratic in them, whatever parametrization is adopted. Such an extrapolation of a known result valid only in specific cases is rather widespread in the literature (see, e.g., Iorio (2011b); Barnes et al. (2013); Johnson et al. (2015)), and may lead to errors when accurate results are looked for. Eqs 8 to 9 are completely general, and can be used with any coordinate system provided that the proper identifications pertaining the angular variables are made.

<sup>2</sup> The replacement  $Q_2 \rightarrow GMJ_2R^2$  must be done in the equations by Iorio (2011c) to obtain the present ones. Other conventions exist in the literature about dimensional quadrupole moments  $Q$ , mainly differing for the sign and the inclusion of  $G$ .

<sup>3</sup> Also the argument of pericenter  $\omega$  and the mean anomaly  $M$  are impacted by  $J_2$  with long-term precessions. We will not display them here because they are not relevant in the present study.

The general relativistic gravitomagnetic field due to the angular momentum  $\mathbf{S}$  of the central body induces the Lense-Thirring effect (Lense & Thirring 1918), whose relevant orbital precessions, valid for an arbitrary orientation of  $\mathbf{S}$ , are<sup>4</sup> (Iorio 2012)

$$\dot{\Omega}_S = \frac{2GS}{c^2 a^3 (1-e^2)^{3/2}} \left[ \hat{S}_z + \cot I (\hat{S}_y \cos \Omega - \hat{S}_x \sin \Omega) \right], \quad (12)$$

$$\dot{I}_S = \frac{2GS}{c^2 a^3 (1-e^2)^{3/2}} (\hat{S}_x \cos \Omega + \hat{S}_y \sin \Omega). \quad (13)$$

In the special case in which  $\mathbf{S}$  is directed along the reference  $z$  axis, Eqs 12 to 13 reduce to the textbook results (Renzetti 2013)

$$\dot{\Omega}_S^{(0)} = \frac{2GS}{c^2 a^3 (1-e^2)^{3/2}}, \quad (14)$$

$$\dot{I}_S^{(0)} = 0. \quad (15)$$

The perspectives of detecting general relativity, mainly in its spin-independent, Schwarzschild-type manifestations, with exoplanets have been studied so far by several authors (Iorio 2006; Adams & Laughlin 2006a,b,c; Heyl & Gladman 2007; Pál & Kocsis 2008; Jordán & Bakos 2008; Ragozzine & Wolf 2009; Iorio 2011a,b; Haranas, Ragos & Mioc 2011; Xie & Deng 2014; Li 2012; Zhao & Xie 2013).

### 3 THE COORDINATE SYSTEM ADOPTED

For consistency reasons with the conventions adopted by Johnson et al. (2015), who, in turn, followed Queloz et al. (2000), the coordinate system used in the present analysis is as follows (see Figure 1).

The line of sight, directed towards the observer, is assumed as reference  $y$  axis, while the  $z$  axis is determined by the projection of the stellar spin axis  $\hat{\mathbf{S}}^*$  onto the plane of the sky, which is inferred from observations. The  $x$  axis is straightforwardly chosen perpendicular to both the other two axes in such a way to form a right-handed coordinate system; it generally does not point towards the Vernal Equinox  $\vee$  at a reference epoch. With the present choice, the coordinate  $\{x, y\}$  plane does not coincide with the plane of the sky which, instead, is now spanned by the  $z$  and  $x$  axes; the  $\{x, y\}$  plane is known as apparent equatorial plane (Queloz et al. 2000). The planetary longitude of the ascending node  $\Omega$  lies in it, being counted from the  $x$  axis to the intersection of the orbital plane with the apparent equatorial plane itself; thus, in general,  $\Omega$  does not stay in the plane of the sky. Moreover, with such conventions, the angle  $I$  between the orbital plane and the coordinate  $\{x, y\}$  plane entering Eqs 8 to 9 and Eqs 12 to 13 is not the orbital inclination  $i_p$ , which refers the plane of the sky and is one of the orbital parameters directly accessible to observations. Instead,  $I$ , which is also the angle from the unit vector  $\mathbf{k}$  of the  $z$  axis to the planetary orbital angular momentum  $\mathbf{L}$ , has to be identified with the angle  $\alpha$  of Queloz et al. (2000). By considering it as a colatitude angle of  $\hat{\mathbf{L}}$  in a spherical coordinate system, the components of the unit vector of

the planetary orbital angular momentum are

$$\hat{L}_x = \sin I \sin \Omega, \quad (16)$$

$$\hat{L}_y = -\sin I \cos \Omega, \quad (17)$$

$$\hat{L}_z = \cos I. \quad (18)$$

In view of Eqs 16 to 18,

$$\frac{d\hat{\mathbf{L}}}{dt} = \frac{\dot{\Omega}_{J_2}^{(0)}}{\cos I} (\hat{\mathbf{L}} \cdot \hat{\mathbf{S}}) \hat{\mathbf{S}} \times \hat{\mathbf{L}}, \quad (19)$$

$$\frac{d\hat{\mathbf{L}}}{dt} = \dot{\Omega}_S^{(0)} \hat{\mathbf{S}} \times \hat{\mathbf{L}}, \quad (20)$$

concisely summarize Eqs 8 to 9 and Eqs 12 to 13. Another angle which is measurable is the projected spin-orbit misalignment  $\lambda$ . It lies in the plane of the sky, and is delimited by the projections of both the stellar spin axis and of the planetary orbital angular momentum. In our coordinate system,  $\lambda$ ,  $i_p$  are the longitude and the colatitude spherical angles, respectively, with  $\lambda$  reckoned from the  $z$  axis to the projection of  $\hat{\mathbf{L}}$  onto the plane of the sky. As such, the components of the planetary orbital angular momentum vector can also be written as

$$\hat{L}_x = \sin i_p \sin \lambda, \quad (21)$$

$$\hat{L}_y = \cos i_p, \quad (22)$$

$$\hat{L}_z = \sin i_p \cos \lambda. \quad (23)$$

In general, both  $I$  and  $\Omega$ , which explicitly enter Eqs 8 to 9 and Eqs 12 to 13, are not directly measurable; they must be expressed in terms of the observable angles  $i_p$ ,  $\lambda$ . To this aim, it is useful to use the unit vector  $\hat{\mathbf{N}}$  directed along the line of the nodes towards the ascending node, which is defined as

$$\hat{\mathbf{N}} = \frac{\mathbf{k} \times \hat{\mathbf{L}}}{|\mathbf{k} \times \hat{\mathbf{L}}|}. \quad (24)$$

From Eqs 21 to 23, its components are

$$\hat{N}_x = -\frac{\cos i_p}{\sqrt{\cos^2 i_p + \sin^2 i_p \sin^2 \lambda}}, \quad (25)$$

$$\hat{N}_y = \frac{\sin i_p \sin \lambda}{\sqrt{\cos^2 i_p + \sin^2 i_p \sin^2 \lambda}}, \quad (26)$$

$$\hat{N}_z = 0. \quad (27)$$

Eqs 16 to 18 and the definition of Equation 24 allow to express the components of  $\hat{\mathbf{N}}$  in terms of  $I$ ,  $\Omega$  as

$$\hat{N}_x = \cos \Omega, \quad (28)$$

$$\hat{N}_y = \sin \Omega, \quad (29)$$

$$\hat{N}_z = 0. \quad (30)$$

<sup>4</sup> The gravitomagnetic pericenter precession, not relevant for us here, will not be shown.

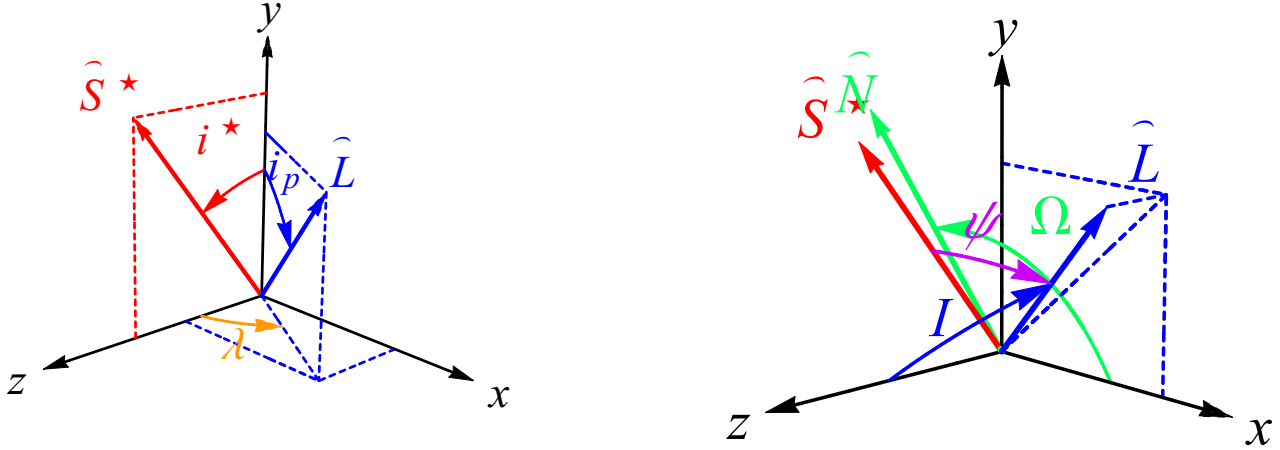


**Figure 1.** The coordinate system adopted. The axes  $x$  and  $z$  span the plane of the sky in such a way that the projection of the stellar spin  $\hat{S}^*$  onto it defines the  $z$  axis. The  $y$  axis is directed along the line of sight towards the observer. The  $\{x, y\}$  plane is the apparent equatorial plane. The inclination of the orbital plane to the plane of the sky is  $i_p$ , while  $i^*$  is the angle between the line of sight and the star’s spin axis. The sky-projected spin-orbit misalignment angle  $\lambda$  lies in the plane of the sky, and is delimited by the projections of  $\hat{S}^*$  and  $\hat{L}$  onto it. The unit vector  $\hat{N}$  of the line of the nodes lies in the apparent equatorial plane perpendicularly to the projection of  $\hat{L}$  onto it. The longitude of the ascending node  $\Omega$  is counted in the  $\{x, y\}$  plane from the  $x$  axis to the line of the nodes. The inclination of the orbital plane to the apparent equatorial plane is  $I$ . The angle between  $\hat{S}^*$  and  $\hat{L}$  is  $\psi$ . The values of the angles used to produce the picture were arbitrarily chosen just for illustrative purposes; they do not correspond to the actual configuration of WASP-33 b.

By adopting the convention<sup>5</sup>  $0 \leq \Omega \leq 2\pi$ , Equation 28 yields<sup>6</sup>

$$\Omega = \arccos \hat{N}_x \text{ for } \hat{N}_y \geq 0, \quad (31)$$

$$\Omega = 2\pi - \arccos \hat{N}_x \text{ for } \hat{N}_y < 0, \quad (32)$$

where  $\hat{N}_x$ ,  $\hat{N}_y$  are expressed in terms of  $i_p$ ,  $\lambda$  by means of Eqs 25 to 26. The inclination  $I$ , defined in the range  $0 \leq I \leq \pi$ , is obtained in terms of  $i_p$ ,  $\lambda$  from

$$I = \arccos (\hat{k} \cdot \hat{L}) \quad (33)$$

and Eqs 21 to 23.

If  $i^*$  is the angle between from the line of sight to  $\hat{S}^*$ , the components of the star’s spin axis in our coordinate system are

$$\hat{S}_x = 0, \quad (34)$$

$$\hat{S}_y = \cos i^*, \quad (35)$$

$$\hat{S}_z = \sin i^*. \quad (36)$$

The angle  $\psi$  between the stellar angular momentum  $\hat{S}^*$  and the planetary orbital angular momentum  $\hat{L}$  can be computed from Eqs 34 to 23 as

$$\hat{S} \cdot \hat{L} = \cos \psi = \cos i_p \cos i^* + \sin i_p \sin i^* \cos \lambda, \quad (37)$$

in agreement with, e.g., Fabrycky & Winn (2009); Iorio (2011b). Incidentally, Equation 37, along with an analogous one which could be straightforwardly obtained from Eqs 16 to 18 and Eqs 34 to 36 in terms of  $I$ ,  $\Omega$ , explicitly shows that the node precession cannot be

generally proportional to  $\cos \psi$ , as previously remarked in Section 2.

Finally, the configurations  $\{i_p, \lambda, i^*\}$  and  $\{\pi - i_p, -\lambda, \pi - i^*\}$  are physically equivalent since they correspond to looking at the planetary system from the opposite sides of the plane of the sky (Masuda 2015). In both case, the angle  $\psi$  remains the same, as explicitly shown by Equation 37. According to Eqs 8 to 9, the node precession remains unaltered, while the rate of  $I$  changes by the amount

$$\begin{aligned} \Delta \dot{I}_{J_2} &\doteq \dot{I}_{J_2}^{\{i_p, \lambda, i^*\}} - \dot{I}_{J_2}^{\{\pi - i_p, -\lambda, \pi - i^*\}} = \\ &= \pm \frac{3n_b J_2 R^2 |\sin \lambda| \cos i^* \sin i_p \cos \psi}{a^2 (1 - e^2)^2 \sqrt{\cos^2 i_p + \sin^2 i_p \sin^2 \lambda}}. \end{aligned} \quad (38)$$

In calculating Equation 38, we used both Equation 31 and Equation 32 in  $\dot{I}_{J_2}^{\{i_p, \lambda, i^*\}}$ ,  $\dot{I}_{J_2}^{\{\pi - i_p, -\lambda, \pi - i^*\}}$  since the transformation  $\{i_p, \lambda\} \rightarrow \{\pi - i_p, -\lambda\}$  changes the sign of  $\hat{N}_y$ , as shown by Equation 26. The  $+$  sign in Equation 38 corresponds to using Equation 32 in  $\dot{I}_{J_2}^{\{i_p, \lambda, i^*\}}$  and Equation 31 in  $\dot{I}_{J_2}^{\{\pi - i_p, -\lambda, \pi - i^*\}}$  while the  $-$  sign is for Equation 31 in  $\dot{I}_{J_2}^{\{i_p, \lambda, i^*\}}$  and Equation 32 in  $\dot{I}_{J_2}^{\{\pi - i_p, -\lambda, \pi - i^*\}}$ .

## 4 CONSTRAINING THE STELLAR SPIN AXIS AND OBLATENESS

### 4.1 Using the precessions of $I$ and $\Omega$

Generally speaking, while the magnitude of the classical precessions driven by the star’s oblateness is at the  $\approx \text{deg yr}^{-1}$  level, the relativistic gravitomagnetic ones about three orders of magnitude smaller. Despite this discrepancy, if, on the one hand, the current

<sup>5</sup> Instead, it seems that Johnson et al. (2015) follow the convention  $-\pi \leq \Omega \leq \pi$ .

<sup>6</sup> Recall that the function  $\arccos$  returns values from 0 to  $\pi$ .

state-of-the-art in the orbital determination of WASP-33 *b* (Johnson et al. 2015), based on data records 5.89 years long (from Nov 12, 2008 to Oct 4, 2014), does not yet allow for a measurement of the relativistic effects, on the other hand, they might exceed the measurability threshold in a not so distant future. Indeed, they are just  $\approx 4 - 8$  times smaller than the present-day errors, which amount to  $\approx 2 - 8 \times 10^{-2} \text{ deg yr}^{-1}$  (Johnson et al. 2015) for the node.

In the following, we will reasonably assume that the measured orbital precessions of WASP-33 *b* are entirely due to the star's oblateness. This will allow us to put much tighter constraints on either  $i^*$  and  $J_2^*$ . Our approach is as follows.

The lucky availability of the measurements of both  $i_p$  and  $\lambda$  at two different epochs some years apart leads to the calculation of the unobservable orbital parameters  $\Omega$ ,  $I$  from Eqs 31 to 33 at the same epochs. According to the measured values of  $i_p$ ,  $\lambda$  by Johnson et al. (2015), it is  $\dot{N}_y < 0$ , so that Equation 32 must be used yielding

$$\Omega^{2008} = 266.4_{-0.2}^{+0.5} \text{ deg}, \quad (39)$$

$$\Omega^{2014} = 268.58_{-0.03}^{+0.04} \text{ deg}. \quad (40)$$

The values by Johnson et al. (2015) differ from Eqs 39 to 40 by  $\pi$ , likely due to the different convention adopted for the node. Since Equation 33 returns

$$I^{2008} = 110.0_{-0.4}^{+0.5} \text{ deg}, \quad (41)$$

$$I^{2014} = 112.9_{-0.7}^{+0.2} \text{ deg}, \quad (42)$$

Eqs 16 to 18 and Eqs 21 to 23 agree both in magnitude and in sign. It is straightforward to compute the average rates of change  $\dot{\Omega}_{\text{exp}}$ ,  $\dot{I}_{\text{exp}}$  by simply taking the ratios of the differences  $\Delta\Omega$ ,  $\Delta I$  of their values at the measurement's epochs to the time span, which in our case is  $\Delta t = 5.89 \text{ yr}$ . Our results are in Table 1.

Eqs 8 to 9 provide us with an accurate mathematical model of the oblateness-driven precessions which, in view of its generality, can be straightforward applied to the present case. Eqs 8 to 9 can be viewed as two functions of the two independent variables  $i^*$ ,  $J_2^*$ . By allowing them to vary within their physically admissible ranges (Iorio 2011b), it is possible to equate  $\dot{\Omega}_{J_2^*}$ ,  $\dot{I}_{J_2^*}$  to  $\dot{\Omega}_{\text{exp}}$ ,  $\dot{I}_{\text{exp}}$  by obtaining certain stripes in the  $\{i^*, J_2^*\}$  plane whose widths are fixed by the experimental ranges of the observationally determined precessions quoted in Table 1. If our model is correct and if it describes adequately the empirical results, the two stripes must overlap somewhere in the considered portion of the  $\{i^*, J_2^*\}$  plane by determining an allowed region of admissible values for the inclination of the stellar spin axis to the line of sight and the star's dimensionless quadrupole mass moment. It is just the case, as depicted in the upper row of Figure 2. From it, it turns that

$$i^* = 142_{-11}^{+10} \text{ deg}, \quad (43)$$

$$J_2^* = (2.1_{-0.5}^{+0.8}) \times 10^{-4}. \quad (44)$$

As a consequence, the angle between the orbital plane and the stellar equator and its precession is as reported in Table 1.

The lower row of Figure 2 depicts the physically equivalent case with  $\pi - i_p$ ,  $-\lambda$ . Now,  $\dot{N}_y > 0$ , and Equation 31 must be used yielding

$$\Omega^{2008} = 86.4_{-0.2}^{+0.5} \text{ deg}, \quad (45)$$

$$\Omega^{2014} = 88.58_{-0.03}^{+0.04} \text{ deg}. \quad (46)$$

While the stripe for  $\dot{\Omega}$  is the same, it is not so for  $\dot{I}$ , as expected from Equation 38; the intersection between the  $\dot{I}$ ,  $\dot{\Omega}$  curves corresponds to

$$\pi - i^* = 38_{-11}^{+10} \text{ deg}. \quad (47)$$

It must be noted that  $J_2^*$  is unchanged.

## 4.2 Constraining the oblateness of Kepler-13 Ab

An opportunity to apply the present method to another exoplanet is offered by Kepler-13 Ab, also known as KOI-13.01 (Szabó et al. 2012; Shporer et al. 2014; Johnson et al. 2014; Masuda 2015). By using the values of its physical<sup>7</sup> and orbital parameters determined with the gravity darkened transit light curves and other observations (Masuda 2015), it is possible to compute analytically the rate of change of  $\cos i_p$  in terms of  $\dot{\Omega}$ ,  $\dot{I}$  by means of Equation 17 and Equation 22, and compare it to its accurately measured value (Masuda 2015) in order to infer  $J_2^*$ . We obtain

$$J_2^* = (6.0 \pm 0.6) \times 10^{-5}, \quad (48)$$

in agreement with Masuda (2015) who seemingly used a different dynamical modelization. We calculated our uncertainty with a straightforward error propagation in our analytical expression of  $J_2^*$  thought as a function of the parameters  $d|\cos i_p|/dt$ ,  $\cos i_p$ ,  $i^*$ ,  $P_b$ ,  $a/R_*$ ,  $\lambda$  affected by experimental uncertainties (Shporer et al. 2014; Masuda 2015).

The definition of the impact parameter

$$b = \left(\frac{a}{R_*}\right) \cos i_p, \quad (49)$$

valid for a circular orbit, along with Equation 17 and Equation 22, allows us to use also the value of  $\dot{b}_{\text{exp}}$  independently measured by Szabó et al. (2012) with the transit duration variation, although it is accurate only to 27%. We get

$$J_2^* = (8.6 \pm 2.4) \times 10^{-5}, \quad (50)$$

which is not in disagreement with Equation 48.

From Equation 49, it turns out that the analytical expressions of  $\dot{b}$  and  $d \cos i_p / dt$  are not independent, so that the availability of independently measured values for both of them do not allow to determine/constrain any further dynamical effect with respect to  $J_2^*$ . Luckily, it seems that other precessions, independent of  $\dot{b}$ ,  $d \cos i_p / dt$ , should be measurable via Doppler tomography in the next years or so (Johnson et al. 2015; Masuda 2015). Depending on the final accuracy reached, such an important measurement will allow, at least in principle, to dynamically measure or, at least, constrain also the stellar spin by means of the Lense-Thirring effect through, e.g.,  $\dot{\lambda}$  calculated with Eqs 12 to 13.

## 5 SUMMARY AND CONCLUSIONS

The use of a general model of the orbital precessions caused by the primary's oblateness, applied to recent phenomenological measurements of some planetary orbital parameters of WASP-33 *b* taken at different epochs 5.89 years apart, allowed us to tightly constrain the inclination  $i^*$  of the spin  $S^*$  of WASP-33 to the line of sight

<sup>7</sup> Contrary to WASP-33 *b*, in the case of Kepler-13 Ab also  $i^*$  is available (Masuda 2015).

**Table 1.** Measured and derived parameters for the WASP-33 system according to Table 1 of Johnson et al. (2015) and the present study. Our values for  $\Omega$ ,  $I$  were inferred by assuming  $0 \leq \Omega \leq 2\pi$ , and calculating Eqs 32 to 33 with the measured values of the orbital inclination  $i_p$  and the sky-projected spin-orbit misalignment angle  $\lambda$  released by Johnson et al. (2015), while the errors were found by numerically determining the maxima and minima of Eqs 32 to 33 thought as functions of  $i_p$ ,  $\lambda$  varying in the rectangle delimited by their measurement errors as per Table 1 of Johnson et al. (2015). The same procedure was adopted for the errors in  $\dot{\Omega}_{\text{exp}}$ ,  $\dot{I}_{\text{exp}}$ , assumed as a function of  $\Omega^{2008}$ ,  $\Omega^{2014}$ ,  $I^{2008}$ ,  $I^{2014}$  varying in the rectangle determined by the errors in them previously calculated. The time span adopted for calculating the precessions is  $\Delta t = 5.89$  yr. The different values of the node quoted by Johnson et al. (2015) with respect to ours are likely due to a different convention adopted by them for the ascending node.

Parameter	(Johnson et al. 2015)	This study
$i_p^{2008}$	$86.61^{+0.46}_{-0.17}$ deg	Same
$i_p^{2014}$	$88.695^{+0.031}_{-0.029}$ deg	Same
$\lambda^{2008}$	$-110.06^{+0.40}_{-0.47}$ deg	Same
$\lambda^{2014}$	$-112.93^{+0.23}_{-0.21}$ deg	Same
$\Omega^{2008}$	$86.39^{+0.49}_{-0.18}$ deg	$266.4^{+0.5}_{-0.2}$ deg
$\Omega^{2014}$	$88.584^{+0.034}_{-0.032}$ deg	$268.58^{+0.04}_{-0.03}$ deg
$\dot{\Omega}_{\text{exp}}$	$0.373^{+0.031}_{-0.083}$ deg yr $^{-1}$	$0.37^{+0.04}_{-0.09}$ deg yr $^{-1}$
$I^{2008}$	–	$110.0^{+0.5}_{-0.4}$ deg
$I^{2014}$	–	$112.9^{+0.2}_{-0.7}$ deg
$\dot{I}_{\text{exp}}$	–	$0.5^{+0.1}_{-0.2}$ deg yr $^{-1}$
$J_2^*$	$[0.54, 3.5] \times 10^{-2}$	$(2.1^{+0.8}_{-0.5}) \times 10^{-4}$
$i^*$	[11.22, 168.77] deg	$142^{+10}_{-11}$ deg
$\psi^{2008}$	–	$99^{+5}_{-4}$ deg
$\psi^{2014}$	–	$103^{+5}_{-4}$ deg
$\dot{\psi}_{\text{exp}}$	–	$0.7^{+1.5}_{-1.6}$ deg yr $^{-1}$

and its dimensionless quadrupole mass moment  $J_2^*$ . Our analytical expressions are valid for arbitrary orbital geometries and spatial orientations of the body’s symmetry axis.

By comparing our theoretical orbital rates of change of the longitude of the ascending node  $\Omega$  and of the inclination  $I$  of the orbital plane with respect to the apparent equatorial plane with the observationally determined ones, we obtained  $i^* = 142^{+10}_{-11}$  deg,  $J_2^* = (2.1^{+0.8}_{-0.5}) \times 10^{-4}$ . Furthermore, the angle between the stellar and orbital angular momenta at different epochs is  $\psi^{2008} = 99^{+5}_{-4}$  deg,  $\psi^{2014} = 103^{+5}_{-4}$  deg. Thus, it varies at a rate  $\dot{\psi} = 0.7^{+1.5}_{-1.6}$  deg yr $^{-1}$ .

In view of the fact that WASP-33 b should transit its host star until 2062 or so and of the likely improvements in the measurement accuracy over the years, such an extrasolar planet will prove a very useful tool for an increasingly accurate characterization of the key physical and geometrical parameters of its parent star via its orbital dynamics. Moreover, also the determination of the general relativistic Lense-Thirring effect, whose predicted size is currently just one order of magnitude smaller than the present-day accuracy level in determining the planetary orbital precessions, may become a realistic target to be pursued over the next decades.

Furthermore, in view of its generality, our approach can be straightforwardly applied to any other exoplanetary system, already

known or still to be discovered, for which at least the same parameters as of WASP-33 b are or will become accessible to the observation. A promising candidate, whose orbital precessions should be measurable via Doppler tomography in the next years, is Kepler-13 Ab. For the moment, we applied our method to it by exploiting its currently known parameters, and we were able to constrain its oblateness in agreement with the bounds existing in the literature.

Finally, in principle, also the periastron, if phenomenologically measurable at different epochs as in the present case, can become a further mean to investigate the characteristics of highly eccentric exoplanetary systems-and to test general relativity as well along the guidelines illustrated here.

## ACKNOWLEDGEMENTS

I would like to thank M. C. Johnson for useful correspondence and clarifications. I am indebted also to an anonymous referee for her/his efforts to improve the manuscript.

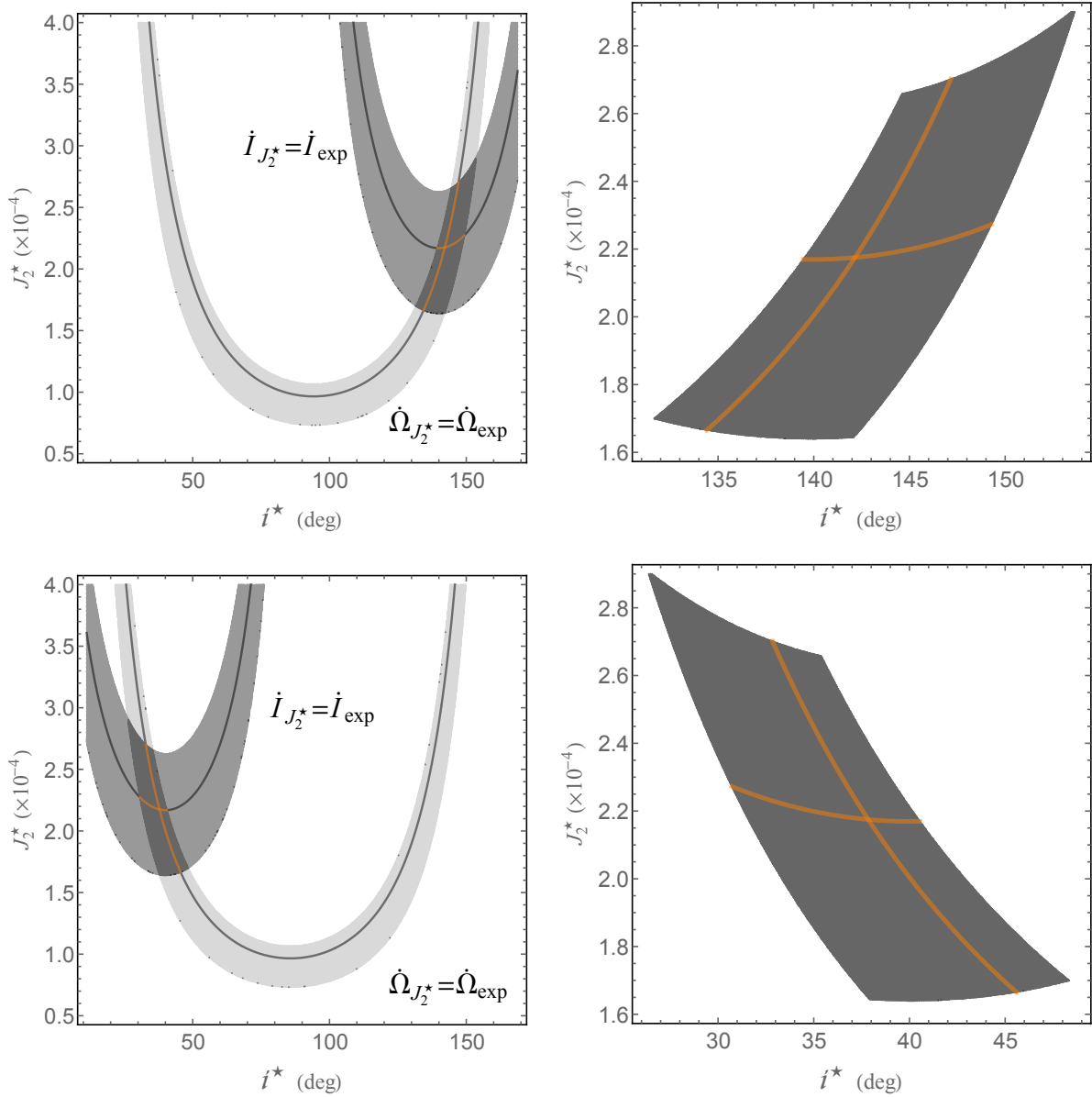


**Figure 2.** Upper row: the darkest region in the plot is the experimentally allowed area in the  $\{i^*, J_2^*\}$  plane, which is enlarged in the right panel. It is determined by the overlapping of the permitted shaded stripes set by the precessions of the node  $\Omega$  and the orbital inclination to the apparent equatorial plane  $I$ . We assumed that the experimental precessions  $\dot{\Omega}_{\text{exp}}$ ,  $\dot{I}_{\text{exp}}$  are entirely due to the stellar oblateness  $J_2^*$ , within the experimental errors. For  $\dot{\Omega}_{J_2^*}$ ,  $\dot{I}_{J_2^*}$ , we used the mathematical model of Eqs 8 to 9 calculated with the values quoted in Table 1; the values for  $R^*$ ,  $M^*$ ,  $a$  were taken from Collier Cameron et al. (2010). The curves inside the shaded areas correspond to the best estimates for  $\dot{\Omega}_{\text{exp}}$ ,  $\dot{I}_{\text{exp}}$ ; their intersection is given by  $i^* = 142$  deg,  $J_2^* = 2.1 \times 10^{-4}$ . Lower row: same as in the upper row, but with  $\pi - i_p$ ,  $-\lambda$ . Note that the stripe for  $\dot{I}$  is different, in agreement with Equation 38. The solution for the stellar spin axis inclination corresponds to  $\pi - i^*$ .

## REFERENCES

- Adams F. C., Laughlin G., 2006a, *Astrophys. J.*, 649, 992  
 Adams F. C., Laughlin G., 2006b, *Astrophys. J.*, 649, 1004  
 Adams F. C., Laughlin G., 2006c, *Int. J. Mod. Phys. D*, 15, 2133  
 Angélie R., Saha P., Merritt D., 2010, *Astrophys. J.*, 720, 1303  
 Barnes J. W., van Eyken J. C., Jackson B. K., Ciardi D. R., Fortney J. J., 2013, *Astrophys. J.*, 774, 53  
 Bertotti B., Farinella P., Vokrouhlick D., 2003, *Physics of the Solar System - Dynamics and Evolution, Space Physics, and Space-time Structure*. Kluwer, Dordrecht  
 Burgay M. et al., 2003, *Nature*, 426, 531  
 Collier Cameron A. et al., 2010, *Mon. Not. Roy. Astron. Soc.*, 407, 507  
 Cook G. E., 1962, *Rep. Prog. Phys.*, 25, 63  
 Cugusi L., Proverbio E., 1978, *Astron. Astrophys.*, 69, 321  
 Damiani C., Rozelot J. P., Lefebvre S., Kilcik A., Kosovichev A. G., 2011, *J. Atm. and Solar-Terrestrial Phys.*, 73, 241  
 Einstein A., 1915, *Sitzungsber. Preuss. Akad. Wiss.*, 47, 831  
 Fabrycky D. C., Winn J. N., 2009, *Astrophys. J.*, 696, 1230  
 Ghez A. M. et al., 2008, *Astrophys. J.*, 689, 1044  
 Gillessen S., Eisenhauer F., Trippe S., Alexander T., Genzel R.,

- Martins F., Ott T., 2009, *Astrophys. J.*, 692, 1075
- Han E., Wang S. X., Wright J. T., Feng Y. K., Zhao M., Fakhouri O., Brown J. I., Hancock C., 2014, *Publ. Astron. Soc. Pac.*, 126, 827
- Haranas I., Ragos O., Mioc V., 2011, *Astrophys. Space Sci.*, 332, 107
- Herbst W., Mundt R., 2005, *Astrophys. J.*, 633, 967
- Heyl J. S., Gladman B. J., 2007, *Mon. Not. Roy. Astron. Soc.*, 377, 1511
- Howard A. W., 2013, *Science*, 340, 572
- Hulse R. A., Taylor J. H., 1975, *Astrophys. J. Lett.*, 195, L51
- Iorio L., 2006, *New Astron.*, 11, 490
- Iorio L., 2011a, *Mon. Not. Roy. Astron. Soc.*, 411, 167
- Iorio L., 2011b, *Astrophys. Space Sci.*, 331, 485
- Iorio L., 2011c, *Phys. Rev. D*, 84, 124001
- Iorio L., 2012, *General Relativity and Gravitation*, 44, 719
- Jackson S., MacGregor K. B., Skumanich A., 2005, *Astrophys. J. Suppl.*, 156, 245
- Johnson M. C., Cochran W. D., Albrecht S., Dodson-Robinson S. E., Winn J. N., Gullikson K., 2014, *Astrophys. J.*, 790, 30
- Johnson M. C., Cochran W. D., Collier Cameron A., Bayliss D., 2015, *Astrophys. J. Lett.*, 810, L23
- Jordán A., Bakos G. Á., 2008, *Astrophys. J.*, 685, 543
- King-Hele D. G., 1962, *Geophys. J. Int.*, 6, 270
- Kozai Y., 1961, *Astron. J.*, 66, 8
- Kramer M. et al., 2006, *Science*, 314, 97
- Lapaz L., 1954, *Publ. Astron. Soc. Pac.*, 66, 13
- Le Verrier U., 1859, *Cr. Hebd. Acad. Sci.*, 49, 379
- Lense J., Thirring H., 1918, *Phys Z.*, 19, 156
- Li L.-S., 2012, *Astrophys. Space Sci.*, 341, 323
- Lucchesi D. M., Peron R., 2010, *Phys. Rev. Lett.*, 105, 231103
- Lucchesi D. M., Peron R., 2014, *Phys. Rev. D*, 89, 082002
- Lyne A. G. et al., 2004, *Science*, 303, 1153
- Masuda K., 2015, *Astrophys. J.*, 805, 28
- Pál A., Kocsis B., 2008, *Mon. Not. Roy. Astron. Soc.*, 389, 191
- Perryman M., 2014, *The Exoplanet Handbook*. Cambridge, UK: Cambridge University Press
- Queloz D., Eggenberger A., Mayor M., Perrier C., Beuzit J. L., Naef D., Sivan J. P., Udry S., 2000, *Astron. Astrophys.*, 359, L13
- Ragozzine D., Wolf A. S., 2009, *Astrophys. J.*, 698, 1778
- Renzetti G., 2013, *Central European Journal of Physics*, 11, 531
- Rozelot J.-P., Damiani C., 2011, *Eur. Phys. J. H*, 36, 407
- Rozelot J. P., Damiani C., Pireaux S., 2009, *Astrophys. J.*, 703, 1791
- Rozelot J. P., Fazel Z., 2013, *Sol. Phys.*, 287, 161
- Shporer A. et al., 2014, *Astrophys. J.*, 788, 92
- Szabó G. M., Pál A., Derekas A., Simon A. E., Szalai T., Kiss L. L., 2012, *Mon. Not. Roy. Astron. Soc.*, 421, L122
- Tarafdar S. P., Vardya M. S., 1971, *Astrophys. Space Sci.*, 13, 234
- Vigneron C., Mangeney A., Catala C., Schatzman E., 1990, *Sol. Phys.*, 128, 287
- Vrbik J., 2005, *Celestial Mechanics and Dynamical Astronomy*, 91, 217
- Wolff S., Simon T., 1997, *Publ. Astron. Soc. Pac.*, 109, 759
- Wolff S. C., Edwards S., Preston G. W., 1982, *Astrophys. J.*, 252, 322
- Xie Y., Deng X.-M., 2014, *Mon. Not. Roy. Astron. Soc.*, 438, 1832
- Zhang F., Lu Y., Yu Q., 2015, *Astrophys. J.*, 809, 127
- Zhao S.-S., Xie Y., 2013, *Res. Astron. Astrophys.*, 13, 1231